JOURNAL OF MATERIALS SCIENCE 26 (1991) 5664–5670

Phosphate glass-ceramic–titanium composite materials

R. ROGIER, F. PERNOT
Laboratoire de Science des Matériaux Vitreux–CNRS, URA 1119, USTL Place E. Bataillon, 34095 Montpellier Cédex 05, France

Phosphate glass-ceramic–titanium particulate composites have been prepared by hot-pressing and their thermal, elastic and mechanical properties have been measured. Results have been then explained using various theoretical models for thermal properties, elasticity and fracture mechanics of particulate composites. It is shown that the thermal and elastic mismatches between glass-ceramic matrix and titanium could produce a microcracking of materials. This microcracking could explain both fracture characteristics and discrepancies between theoretical and experimental values of elastic moduli.

1. Introduction

Composite materials have been a subject of intensive interest during the last four decades. The goal for development of such materials has been to achieve a combination of properties not achievable by any of the elemental materials acting alone. Many potential applications exist for these materials, such as military devices, wear-resistant materials, internal combustion engine parts and biomedical materials [1].

In this last field, calcium alumino-phosphate glass-ceramic–metal particulate composites have been proposed to act as thermal and elastic graded seals between various dense metal cores of prostheses and a porous phosphate glass-ceramic coating [2, 3].

While composites have been used in engineering applications, the operating conditions under which such materials have to function led to the science of composite materials. That means fundamental studies on interactions between components: matrix, reinforcement and particularly the role of the interface [4]. It also deals with the basic understanding of deformation behaviour, strength and toughness.

In all these fields, a lot of work has thus been already performed on glass–glass, ceramic–glass or glass–metal particulate composites. Most studies have dealt with the strength-controlling factor and/or the effect of microcracking on elastic behaviour [5–11]. However, these parameters have hardly yet been studied for the phosphate glass-ceramic–metal composites previously proposed for orthopaedic applications [2, 12]. Only their method of synthesis has been investigated in detail. Their thermal and elastic properties have been measured, mainly to ensure that they lay within those of the phosphate glass-ceramic matrix and those of the corresponding metallic reinforcement (titanium, 316 L stainless steel, cobalt chromium 788 alloy).

It has therefore turned out that detailed studies on thermal and elastic behaviour and fracture mechanics of these composites would be useful for a better knowledge of these materials. This paper deals with phosphate glass-ceramic–titanium composites.

2. Materials and experimental procedure

2.1. Base products and preparation of composites

The parent calcium alumino-phosphate (CAP) glass is prepared from a mixture of calcium bis-dihydrogen phosphate and hydrated aluminium orthophosphate. It is melted in a Pt–10% Rh crucible at 1300 °C for 2 h, then crushed into a powder with a particle size lower than 50 μm. Titanium is a commercial product (Baudier-Poudmet). The composition and properties of parent glass, glass-ceramic and titanium are summarized in Table I.

Seven mixtures of CAP glass with increasing volume fractions (from 3.5 to 50%) of titanium particles are vacuum-hot-pressed into composite discs of about 5 mm thickness. The "flash pressing" method is used; details have been given in previous papers [2, 13]. Pressure is removed as soon as samples are totally sintered. They are then kept at 700 °C for 1 h to obtain total ceramization of the matrix. Two or three discs of each composition are thus prepared.

2.2. Methods of measurement

2.2.1. Thermal properties

Linear thermal expansion is measured with a differential dilatometer (D.I. 10-2, Adamel-Lhomargy) using vitreous silica as reference material. Measurements are made from room temperature to 750 °C, at a linear heating rate of 3 °C min^{-1}. From the recorded curves, one can deduce [2]:

(i) the relative expansion $\Delta L/L_0$ of the samples at each temperature, and

(ii) the average linear thermal expansion coefficient $\alpha_{T_2-T_1}$ between two temperatures T_1 and T_2.

0022–2461/91 $03.00 + .12

TABLE I Composition and properties of materials for the preparation of CAP glass-ceramic–titanium composites

Composition and properties	CAP glass	CAP glass-ceramic	Titanium
Composition (wt %)			
P_2O_5	69	69	–
CaO	22.7	22.7	–
Al_2O_3	8.3	8.3	–
Ti	–	–	$\geqslant 96$
Density ($g\,cm^{-3}$)	2.64	2.65	4.5
Average linear expansion coefficient ($10^6\,°C^{-1}$)			
α_{20-500}	9.3	16.7	8.9
α_{20-700}	–	16.4	9.0
Young's modulus (GPa)	64	68	110
Poisson's ratio	0.256	0.180	0.340
Fracture stress (MPa)	53.9	146.7	536 $\sigma_Y = 454$
Fracture toughness ($MPa\,m^{1/2}$)	0.78	2.22	–
Average radius of particles (μm)	$\leqslant 50$	–	10

2.2.2. Elastic properties

Elastic properties are determined using a resonance dynamic method based on the magnetostrictive effect [2, 14]. The specimen resonators may be chosen either as square-shaped bars or discs. Only Young's modulus can be measured using square-shaped bars; discs are used for the determination of both Young's modulus and Poisson's ratio. The knowledge of two elastic constants allows one to calculate the others [2, 15].

2.2.3. Mechanical properties

Flexural strength σ_R is measured on 1.5 mm × 3 mm × 15 mm bars. They are tested in three-point bending with a 12 mm span in an Instron machine operating at a loading rate of 0.1 mm min^{-1}. All measurements are made in air at room temperature. For each composite, seven to sixteen specimens are fractured.

With 2 mm × 4 mm × 24 mm bar specimens, fracture toughness K_{IC} is determined using the three-point bend test of a single-edge notched bend (SENB) specimen over a 16 mm span. A notch as thin as possible of about 1.3 mm depth is machined at the midpoint of one 24 mm edge of each specimen.

Samples (two to nine for each composite) are tested at a crosshead speed of 0.05 mm min^{-1}. All measurements are carried out in air at room temperature.

Fracture toughness is calculated from specimen dimensions, notch depth and fracture load [2, 16]. As was shown previously [16, 17], such conditions allow one to reach the "true" K_{IC} factor. It has also to be noticed that the SENB technique gives an initiation toughness [16, 18, 19].

The knowledge of K_{IC} and σ_R allows calculation of other mechanical characteristics: critical flaw size a_c and fracture energy Γ.

Critical flaw size (the size of the defect from which the fracture starts) may be obtained from [20, 21]

$$a_c = \left(\frac{Z}{Y}\frac{K_{IC}}{\sigma_R}\right)^2 \quad (1)$$

where Y is a dimensionless term that depends on the crack depth and the test geometry [16], and Z is another dimensionless quantity that depends on the configuration of the crack [20]. For a straight through-thickness crack (Griffith flaw) [22, 23]

$$\left(\frac{Z}{Y}\right)^2 = \frac{1}{1.21\,\pi}$$

For a penny-shaped crack [22, 24]

$$\left(\frac{Z}{Y}\right)^2 = \frac{2}{\pi}$$

In the case of plane strain, Γ is given by [10]

$$\Gamma = \frac{K_{IC}^2}{2E}(1 - \nu^2) \quad (2)$$

where E = Young's modulus and ν = Poisson's ratio. Since Γ is directly calculated from K_{IC} determined by the SENB method, it is also an initiation energy and does not take into account energy-dissipative mechanisms, which occur during fracture propagation.

To use this equation, it is previously necessary to ensure that a condition of plane strain is really obtained and also that the strain cannot be relieved by general plastic deformation. These conditions are fulfilled if [17, 23]

$$a \geq 2.5\left(\frac{K_{IC}}{\sigma_Y}\right)^2 \quad \text{and} \quad b \geq 2.5\left(\frac{K_{IC}}{\sigma_Y}\right)^2 \quad (3)$$

where σ_Y = yield stress.

The ratio K_{IC}/σ_Y is generally a very small number for ceramic materials due to limited plasticity [19] and also for such composites [25] these equations are thus nearly always satisfied.

3. Results and discussion

3.1. Thermal properties

The expansion curves of titanium composites (Fig. 1) show a shoulder between 100 and 200 °C which is due to $\alpha \rightarrow \beta$ transformation of the $AlPO_4$ cristobalite form [26–28]. Sometimes, other features occur at higher temperatures. As an example, expansion of 20 and 37% titanium composites increases sharply from about 700 °C (Fig. 1). This could be due to a foaming produced by gas emanating from titanium at high temperature.

The average linear thermal expansion coefficients have been calculated between 20 and 500 °C, 20 and 700 °C respectively. They decrease as a function of titanium volume fraction, c_p, since α_{Ti} is much lower than α_{CAP} (Table I).

Most experimental values of α_{20-500} lie within the curves of Turner [29, 30] and Kerner [30, 31], which predict theoretical evolutions of α as a function of c_p and in terms of the thermal and elastic properties of the components (Fig. 2a). Some values of α_{20-700} lie

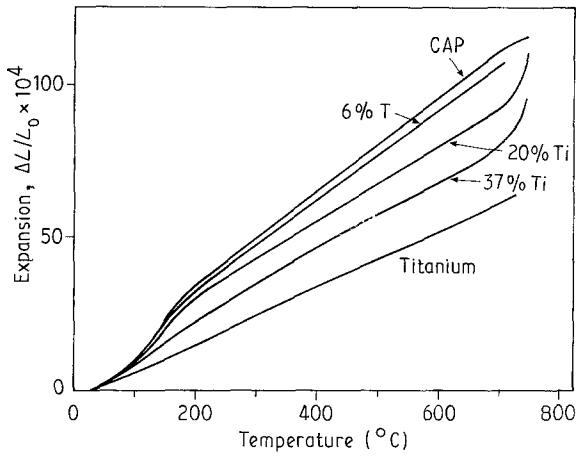

Figure 1 Linear thermal expansion of CAP glass-ceramic–titanium composites.

below the Turner lower bound (Fig. 2b); they correspond to samples which have an expansion curve showing features at high temperature.

3.2. Elastic properties

Young's modulus increases with the volume fraction, c_p, of titanium. The experimental results (Table II) have been compared with values given by various models. These expressions predict the theoretical evolution of Young's modulus of composites as a function of the volume fraction of the second phase and from the elastic properties of individual components [7, 31–34]. Most of them assume that strains and stresses are totally transferred from one phase to the other, which requires both a close contact between matrix and particles and no microcracking of materials. These models have representative curves lying within two limits. The upper-bound Voigt model [32] assumes that the composite solid is behaving as a constant-strain system. The lower-bound Reuss model [33] considers the composite as a constant-stress system.

Fig. 3 shows that most experimental values fall below Reuss's lower bound, which means that one or both conditions noticed above are not fulfilled in the glass-ceramic–titanium system.

In these composites, the coefficient of thermal expansion of the matrix is much higher than that of titanium (Table I). A residual stress field is developed within and around particles as the body cools from ceramization (700 °C) to room temperature (20 °C). Assuming titanium particles as spherical, each of them

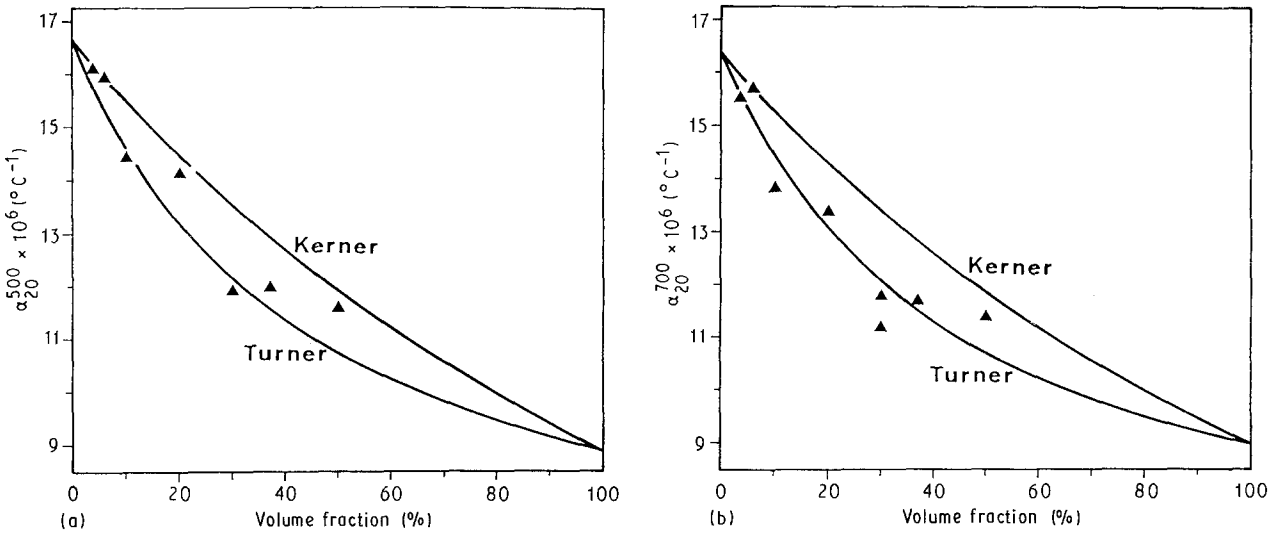

Figure 2 (a, b) Theoretical and experimental average linear thermal expansion coefficients of CAP glass-ceramic–titanium composites.

TABLE II Elastic and mechanical properties of CAP glass-ceramic–titanium composites

Titanium fraction (vol %)	Young's modulus (GPa)	Poisson's ratio	Fracture stress (MPa)	Fracture toughness (MPa m$^{1/2}$)	Critical flaw size (μm)		Mean free path (μm)
					Griffith flaw	Penny-shaped crack	
0	68	0.180	146.7	2.22	60	145	–
3.5	69.5	0.185	154.9	2.47	67	162	368
6	70	0.199	149.5	2.40	68	164	209
10	71	0.195	157.7	2.39	60	145	120
20	71.5	0.203	122	2.24	89	215	53
30	73	0.209	122.1	2.14	81	196	31
37	77	0.220	123.3	2.32	93	225	23
50	80	0.229	121.1	2.38	101	244	13

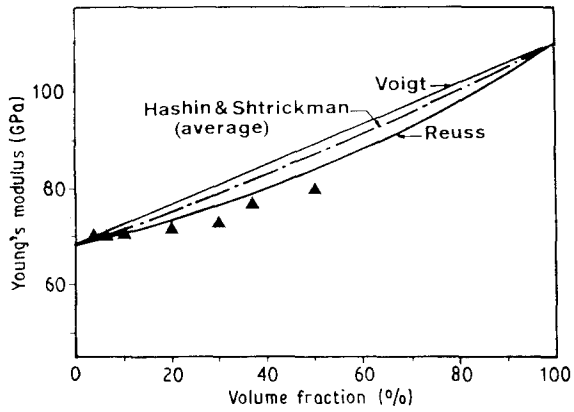

Figure 3 Theoretical and experimental Young's modulus of CAP glass-ceramic–titanium composites.

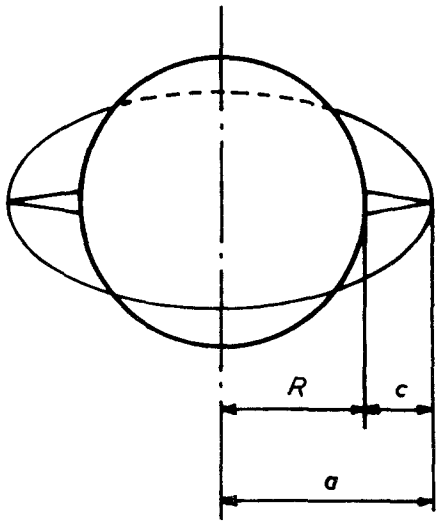

Figure 4 An annular flaw associated with a spherical particle under thermoelastic stress (from Krstic and Vlajic [36]).

will be subjected to a uniform hydrostatic pressure, which can be estimated by [35]

$$P_0 = \Delta\alpha\Delta T\left(\frac{1+\nu_m}{2E_m} + \frac{1-2\nu_p}{E_p}\right)^{-1} \quad (4)$$

where $\Delta\alpha = \alpha_m - \alpha_p$, ΔT = difference between ceramization and room temperature (680 °C), ν_m, ν_p = Poisson's ratio of matrix and particles, respectively, and E_m, E_p = Young's modulus of matrix and particles, respectively. Substituting reported values from Table I into Equation 4 then gives

$$P_0 = 434\ \text{MPa}$$

This pressure probably ensures the contact between matrix and particles. However, thermal and elastic mismatches between both phases also induce radial stress σ_{rr} and tangential stress $\sigma_{\theta\theta}$ in the matrix [10, 36]:

$$-\sigma_{rr} = 2\sigma_{\theta\theta} = P_0\left(\frac{R}{r}\right)^3 \quad (5)$$

where R = radius of the particle and r = distance from the centre of the particle.

The tangential stress outside particles, if sufficiently high, can initiate radial cracks originating from the particle–matrix interfaces [5, 10, 36–38]. This microcracking could thus explain the fall in Young's moduli [11, 39], provided it eventually occurs.

The possibility of crack initiation is governed by the magnitude of the stress intensity factor, K_I, at the cracks associated with the particles. If K_I exceeds the critical value K_{ICm} for the matrix, then the cracks will extend. K_I can be estimated using the analysis of Krstic and Vlajic [36].

In this analysis, each radial crack is considered to be a part of a major crack, i.e. a part of the total crack length, which consists of the length of the cavity in which the particle is embedded and a small annular crack (Fig. 4). It is then assumed that the crack is kept open by the uniform thermoelastic stress, P_0, which acts along the particle–matrix interface and by a diminishing tangential stress, which acts on annular crack surfaces. The total stress intensity factor, K_I, is thus found to be a function of the particle size, R, the level of internal stress, P_0 and the ratio of the grain to flaw size, R/a, as given by the expression [36]

$$K_I = \frac{2P_0R^{1/2}}{\pi^{1/2}}\left\{\left(\frac{R}{a}\right)^{-1/2}\left[1-\left(1-\frac{R^2}{a^2}\right)^{1/2}\right] + \frac{1}{2}\left(\frac{R}{a}\right)^{3/2}\left(1-\frac{R^2}{a^2}\right)^{1/2}\right\} \quad (6)$$

Rearranging Equation 6, a critical grain size R_c, below which crack initiation cannot occur, can be deduced:

$$R_c = \frac{\pi K_I^2}{4P_0^2}\left\{\left(\frac{R}{a}\right)^{-1/2}\left[1-\left(1-\frac{R^2}{a^2}\right)^{1/2}\right] + \frac{1}{2}\left(\frac{R}{a}\right)^{3/2}\left(1-\frac{R^2}{a^2}\right)^{1/2}\right\}^{-2} \quad (7)$$

Equations 6 and 7 assume that a cannot be lower than R. In other words, the ratio R/a of grain to flaw size cannot be higher than unity. Assuming that R/a tends to this limit, then

$$[K_I]_{lim} = \frac{2P_0R^{1/2}}{\pi^{1/2}} \quad (8a)$$

or

$$[R_c]_{lim} = \frac{\pi K_I^2}{4P_0^2} \quad (8b)$$

Substituting reported values for the glass-ceramic–titanium system, i.e. $P_0 = 434$ MPa and $K_I = K_{ICm} = 2.22\ \text{MPa m}^{1/2}$, then Equation 8b gives

$$[R_c]_{lim} = 20.5\ \mu\text{m}$$

Crack initiation should not occur since measurement of the average titanium particle size by laser granulometry gives 10 μm. This could be the reason why microcracks have never been observed. However, dropping of elastic moduli could not then be easily explained.

In practice, titanium particles are not spherical; their sharp-cornered shape could increase stress concentrations at the angles and their size could have been underestimated by the method of measurement, which gives an equivalent spherical diameter (ESD). In the microcracking mechanism, such a diameter is not necessarily the best value to consider since it never

relates to the true major particle dimension [40]. Moreover, the glass-ceramic matrix is not homogeneous at a microscopic scale. These assumptions can be translated in terms of Equation 8:

(i) Increase in stress concentrations at the angles amounts to local enhancements of P_0.

(ii) The effective particle radius really reaches more than 10 μm.

(iii) The use of K_{ICm} measured for the matrix assumes that perturbations due to the microstructure are negligible, which is not necessarily valid. It has been shown that the K_{IC} measured with a large flaw can be much higher than the local effective critical stress intensity factor [41, 42].

Plots of $[K_I]_{lim}$ as a function of R_c for various P_0 values (Fig. 5) show that, for $[R_c]_{lim}$ equal to 10 μm:

(i) P_0 should reach more than 622 MPa, if K_I is taken equal to the critical stress intensity factor measured for the matrix (2.22 MPa $m^{1/2}$).

(ii) A pressure P_0 of 434 MPa leads to a $[K_I]_{lim}$ of 1.55 MPa $m^{1/2}$. K_{ICm} should then be divided by at least 1.5. This is not unrealistic since a ratio of more than 3 has already been found, in ceramic materials, between the stress intensity factor and the local effective critical stress intensity factor [41].

Therefore, microcracking has every chance to occur; it is likely to be due to one or more of the causes previously described. Once microcracks have been initiated, the increase of a (decrease of R/a) induces a rapid decrease of K_I (Fig. 6), which no longer reaches the effective K_{ICm}; the crack is then arrested. As an example, assuming an effective radius of 15 μm, local pressure P_0 of 500 MPa and K_{ICm} of 2 MPa $m^{1/2}$, Fig. 6 shows that the crack is arrested as soon as R/a is 0.98 (close to unity). The length c of the annular crack beyond the particle–matrix interface (Fig. 4) is then not higher than 0.31 μm. It is still too small to be seen by optical microscopy.

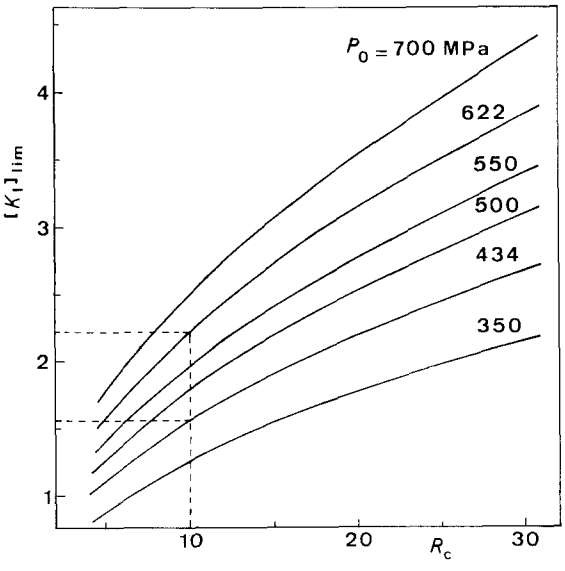

Figure 5 The variation of limiting stress intensity factor with radius of particles for various pressures.

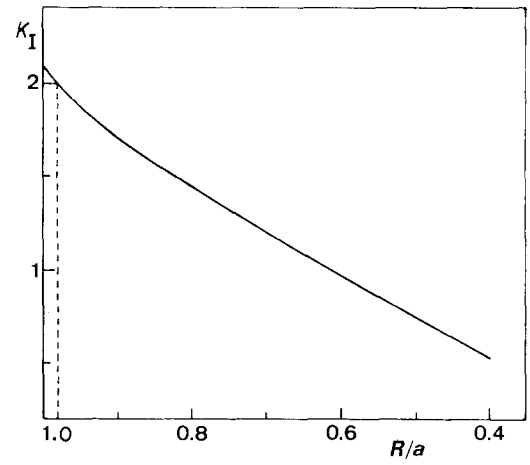

Figure 6 The stress intensity factor as a function of relative crack length. R = 15 μm, P_0 = 500 MPa.

The presence of microcracks has thus been detected indirectly by elastic modulus measurements [39]. It is then interesting to calculate the microcrack density, N_m, corresponding to the decrease of E. For a random array of penny-shaped cracks of radius a, it has been shown that Young's modulus is given by [11, 39]

$$E = E_0\left(1 + \frac{16}{9}N_m a^3\right)^{-1} \quad (9)$$

where E_0 = Young's modulus of the uncracked material. Introducing R/a in Equation 9 and rearranging:

$$N_m = \frac{9}{16R^3}\left(\frac{R}{a}\right)^3\left(\frac{E_0}{E} - 1\right) \quad (10)$$

This density is compared with the number of titanium particles N_{Ti} per unit volume, which is estimated from the formula for a random dispersion of equally sized spheres, radius R [39]:

$$N_{Ti} = \frac{3c_p}{4\pi R^3} \quad (11)$$

where c_p = volume fraction of particles. Dividing Equation 10 by Equation 11

$$\frac{N_m}{N_{Ti}} = \frac{3\pi}{4c_p}\left(\frac{R}{a}\right)^3\left(\frac{E_0}{E} - 1\right) \quad (12)$$

Fig. 7a and b show the evolution of N_m and N_m/N_{Ti} as a function of c_p for R equal to 15 μm and R/a to 0.98, and assuming that E_0 corresponds to the average between upper and lower bounds of the Hashin and Shtrickman model [34].

3.3. Mechanical properties

Mechanical properties (Table II) have been studied as a function of titanium volume fraction c_p. The variations have been related to results deduced from the studies of elastic properties.

The evolution of fracture toughness and fracture energy (Fig. 7c and d) can be related both to that of the microcrack density N_m (Fig. 7a) and the ratio N_m/N_{Ti} (Fig. 7b), and interpreted in terms of the suggestions of Miyata *et al.* [43].

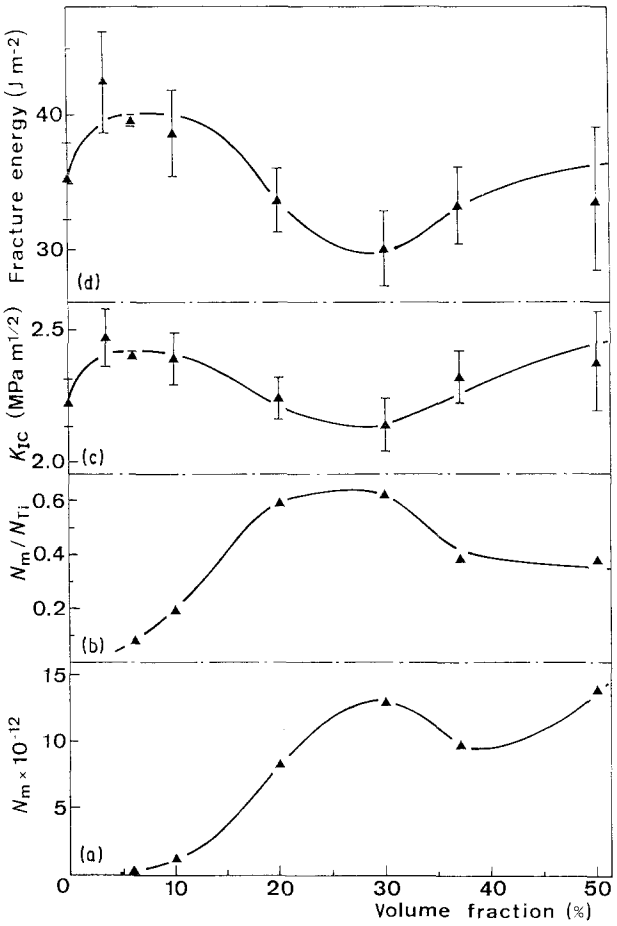

Figure 7 Fracture properties of CAP glass-ceramic–titanium composites: (a) density of microcracks; (b) ratio of microcrack density to the number of titanium particles per unit volume; (c) fracture toughness; (d) fracture energy.

The initial increase up to 3.5%, then the constancy up to 10% can be explained by the low density of pre-existing microcracks in this region. The energy absorption mechanisms consist essentially of stress-induced microcrack formation rather than propagation of pre-existing microcracks. In such a case, the increase in K_{IC} is not very important. At the same time, the strength shows a slight increase (Fig. 8) due to the higher elastic modulus of the dispersed phase and also to the introduction of the matrix–particle interface. However, these effects are negligibly small [43]. Microcrack coalescence has little chance to occur and fracture is probably due to an inherent critical flaw in the matrix, the size of which is in Table II for various configurations.

From 20% inclusions, the microcrack density becomes high (6 to 10 times higher than previously) and the ratio N_m/N_{Ti} reaches more than 60% (Fig. 7a and b). The high density of microcracks combined with the decrease of interparticle spacing (taken equal to the mean free path: see Table II of Fullman [44]) makes it easier to propagate the primary crack by the microcrack–microcrack and primary crack–microcrack coalescence mechanisms [43]. Then K_{IC} and Γ reach the lowest values (Fig. 7c and d). From this volume percentage of 20%, subcritical inherent flaw–microcrack or microcrack–microcrack linking can also occur prior to catastrophic failure [20, 42]. The strength is then determined either by the extension of a flaw

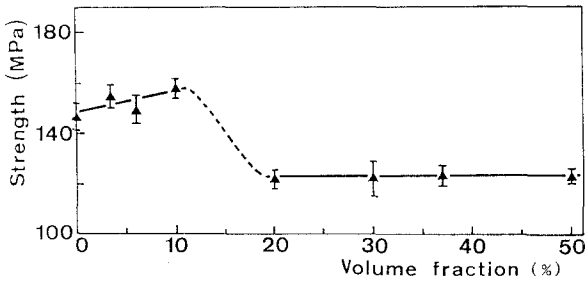

Figure 8 Fracture stress of CAP glass-ceramic–titanium composites.

larger than the initial inherent flaw [20] or by interaction and coalescence of multiple microscopic cracks [42]. As a result, the curve of the strength (Fig. 8) exhibits a discontinuity between 10 and 20% inclusions, due to the change in the fracture mechanism. From this last volume percentage, σ_R remains nearly constant at a value lower than the fracture stress of glass-ceramic (Fig. 8) and the calculated critical flaw size (true [20] or apparent [42]) increases sharply (Table II).

Beyond 30% inclusion, the microcrack density no longer increases significantly. The ratio N_m/N_{Ti} decrease from 60 to 40% while the average distance between particles still decreases (Table II). The linking mechanism then requires that the isolated microcracks propagate round particles to join inherent flaws or other microcracks. This new energy absorption process, known as a "high energy crack-propagation process" [45], again increases K_{IC} and Γ. However, inherent flaw–microcrack or microcrack–microcrack coalescence mechanisms are always subcritical. Fracture occurs for the same true or apparent critical flaw size as previously and σ_R does not increase again (Fig. 8).

4. Conclusion

Glass-ceramic–titanium composites could be obtained from mixtures of a calcium alumino-phosphate parent glass and various volume fractions (up to 50%) of titanium particles. They have been prepared by hot-pressing using the "flash pressing" technique.

Their elastic moduli measured by dynamic methods have been found lower than values given by most theoretical expressions, which has led to the conclusion that microcracking occurs in these composites. Such a phenomenon allows us to explain both elastic and mechanical properties. However, crack initiation has been assumed to originate from the particle–matrix interface and described using the analysis of Krstic and Vlajic [36]. It has also been considered as a spontaneous phenomenon due to thermal and elastic mismatches alone. In this context, some additional causes of microcracking have had to be assumed as accompanying the mismatches: underestimation of particle radius, local increase of hydrostatic pressure and local decrease of critical stress intensity factor.

Some other mechanisms could still be considered, relating to the true effect of the matrix. Anisotropies between its two crystalline phases ($AlPO_4$ and $Ca(PO_3)_2$) [3, 46, 47] should be considered [42]. It is

also well known that phase transformations can introduce stresses; in the present case ceramization of the vitreous phase into glass-ceramic [48] and $\alpha \rightarrow \beta$ transformation of $AlPO_4$. Moreover after ceramization, materials are cooled directly to room temperature without any annealing treatment, which could also produce stresses. Considering all these stresses acting as an applied stress, the equation of Krstic and Vlajic could be modified to introduce this additional stress [49], which increases the probability of crack initiation.

Another possibility would consist of assuming that microcracking occurs inside the matrix. The pressure due to thermal mismatch would play the role of the applied stress [49]. It would then produce either a propagation of pre-existing microcracks in the matrix or formation of microcracks under this additional applied stress. In both cases a fall of elastic modulus would be observed due to an increase either of the crack size or microcrack density (Equation 9). Checks of these hypotheses would need to have more data about the matrix itself.

The analysis of Krstic and Vlajic gives a satisfactory explanation of the observed phenomena; however, it is based on an axisymmetrical stress distribution, which is not necessarily the best approximation to assume for later local variations of hydrostatic pressure or toughness. Theories based on cracks occurring at preferred locations of the particle–matrix interface or in its vicinity [50, 51] would then be perhaps more suitable.

All these new hypotheses to explain microcrack formation will be the object of subsequent investigations. However, it is already interesting to note that, whatever the hypotheses on microcracking, once it is assumed, its consequences for elastic and mechanical properties will not be modified significantly with respect to those described in this paper.

References

1. J. J. MECHOLSKY, *Amer. Ceram. Soc. Bull.* **65** (1986) 315.
2. R. ROGIER and F. PERNOT, *Materials in Medicine*, in press.
3. F. PERNOT, J. ZARZYCKI, F. BONNEL, P. RABISCHONG and P. BALDET, *J. Mater. Sci.* **14** (1979) 1694.
4. A. G. METCALFE, in "Composite Materials", Vol. 1, edited by A. G. Metcalfe (Academic, New York, 1974) p. 1.
5. D. B. BINNS, in "Science of Ceramics", Vol. 1, edited by G. H. Stewart (Academic, New York, 1962) p. 315.
6. R. W. DAVIDGE and T. J. GREEN, *J. Mater. Sci.* **3** (1968) 629.
7. F. F. LANGE, in "Composite Materials", Vol. 5, edited by L. J. Broutman (Academic, New York, 1974) p. 1.
8. J. C. SWEARAGEN, E. K. BEAUCHAMP and R. J. EAGAN, in "Fracture Mechanics of Ceramics", Vol. 4, edited by R. C. Bradt, D. P. H. Hasselman and F. F. Lange (Plenum, New York, 1978) p. 973.
9. A.K. KHAUND and P. NICHOLSON, *J. Mater. Sci.* **15** (1980) 177.
10. N. MIYATA and H. JINNO, *ibid.* **16** (1981) 2205.
11. D. P. H. HASSELMAN and J. P. SINGH, *Amer. Ceram. Soc. Bull.* **50** (1977) 559.
12. R. ROGIER and F. PERNOT, in "Handbook of Bioactive Ceramics", Vol. 1, edited by T. Yamamuro, L. L. Hench and J. Wilson (CRC Press, Boca Raton, 1990) p. 183.
13. M. DECOTTIGNIES, J. PHALIPPOU and J. ZARZYCKI, *J. Mater. Sci.* **13** (1978) 2605.
14. J. F. W. BELL and J. M. PELMORE, *J. Phys. E: Sci. Just.* **10** (1977) 1145.
15. D. E. GRENOBLE, J. L. KATZ, K. L. DUNN, R. S. GILMORE and K. LINGA MURTY, *J. Biomed. Mater. Res.* **6** (1972) 221.
16. W. F. BROWN and J. E. SRAWLEY, in ASTM Special Technical Publication No. 410 (American Society for Testing and Materials, Baltimore, 1967) p. 1.
17. J. L. CHERMANT, F. OSTERSTOCK and G. VADAM, *Verres Réfract.* **33** (1979) 843.
18. R. W. DAVIDGE and G. TAPPIN, *J. Mater. Sci.* **3** (1968) 165.
19. A. G. EVANS, in "Fracture Mechanics of Ceramics", Vol. 1, edited by R. C. Bradt, D. P. H. Hasselman and F. F. Lange (Plenum, New York, 1974) p. 17.
20. A. G. EVANS and G. TAPPIN, *Proc. Br. Ceram. Soc.* **23** (1972) 275.
21. J. PHALIPPOU, T. WOIGNIER and R. ROGIER, *J. Phys.* **24** (1989) C4.
22. R. PABST, *Z. Werkstofftech.* **6** (1975) 17.
23. J. L. CHERMANT and F. OSTERSTOCK, *J. Mater. Sci.* **11** (1976) 1939.
24. D. J. GREEN, P. S. NICHOLSON and J. D. EMBURY, *ibid.* **14** (1979) 1413.
25. N. MIYATA and H. JINNO, *ibid.* **17** (1982) 547.
26. A. J. LEADBETTER and T. W. SMITH, *Phil. Mag.* **33** (1976) 105.
27. V. G. KOMLEV, I. D. KURKINA and V. A. PETROV, *Ogneupory* **12** (1979) 46.
28. W. F. HORN and F. A. HUMMEL, *J. Amer. Ceram. Soc.* **63** (1980) 338.
29. P. S. TURNER, *J. Res. Nat. Bur. Stand.* **37** (1946) 239.
30. S. J. FELTHAM, B. YATES and R. J. MARTIN, *J. Mater. Sci.* **17** (1982) 2309.
31. E. H. KERNER, *Proc. Phys. Soc. B* **69** (1956) 808.
32. W. VOIGT, "Lehrbuch der Kristallophydik" (Teubner, Berlin, 1910).
33. W. REUSS, *Z. Angew. Math. Mech.* **9** (1929) 49.
34. Z. HASHIN and S. SHTRIKMAN, *J. Mech. Phys. Solids* **11** (1963) 127.
35. J. SELSING, *J. Amer. Ceram. Soc.* **44** (1961) 419.
36. V. D. KRSTIC and M. D. VLAJIC, *Acta Metall.* **31** (1983) 139.
37. F. F. LANGE, in "Fracture Mechanics of Ceramics", Vol. 2, edited by R. C. Bradt, D. P. H. Hasselman and F. F. Lange (Plenum, New York, 1983) p. 599.
38. D. J. GREEN, *J. Amer. Ceram. Soc.* **64** (1981) 138.
39. *Idem, ibid.* **65** (1982) 610.
40. B. R. JENNINGS and K. PARSLOW, *Proc. R. Soc.* **A419** (1988) 137.
41. R. W. RICE, S. W. FREIMAN and J. J. MECHOLSKI Jr, *J. Amer. Ceram. Soc.* **63** (1980) 129.
42. T. OKADA and G. SINES, *ibid.* **66** (1983) 719.
43. N. MIYATA, K. TANIGAWA and H. JINNO, in "Fracture Mechanics of Ceramics", Vol. 5, edited by R. C. Bradt, D. P. H. Hasselman and F. F. Lange (Plenum, New York, 1983) p. 609.
44. R. L. FULLMAN, *Trans. AIME, J. Met.* **197** (1953) 447.
45. N. MIYATA and H. JINNO, *J. Mater. Sci.* **7** (1972) 973.
46. F. PERNOT and A. KHADOM-RASHID, in "Advances in Biomaterials", Vol. 8, edited by C. de Putter *et al.* (Elsevier, Amsterdam, 1988) p. 387.
47. R. W. RICE, R. C. POHANKA and W. J. McDONOUGH, *J. Amer. Ceram. Soc.* **63** (1980) 703.
48. J. J. MECHOLSKI, in "Fracture Mechanics of Ceramics", Vol. 6, edited by R. C. Bradt, D. P. H. Hasselman and F. F. Lange (Plenum, New York, 1983) p. 165.
49. V. D. KRSTIC, *J. Amer. Ceram. Soc.* **67** (1984) 589.
50. A. G. EVANS, *J. Mater. Sci.* **9** (1974) 1145.
51. M. V. SWAIN, *ibid.* **16** (1981) 151.

Received 23 July 1990
and accepted 6 February 1991